DOI: 10.1093/mnras/stac1884

Low-pressure and low-temperature phase equilibria applied to Pluto's lower atmosphere

Sugata P. Tan*

Planetary Science Institute, Tucson, AZ, U. S. A.

ABSTRACT

While phase equilibria at conditions on Pluto's surface have been studied, the fate of the equilibria in the lower atmosphere as the altitude increases has not. In this study, the gravitational effect is included in the thermodynamic modeling so that not only the deposition point can be located, but also the vertical pressure and density profiles below the deposition point can be determined along with the corresponding compositional profiles in the equilibrium phases. The non-ideality of vapour-solid phase equilibria at low pressures and temperatures is also discussed for Pluto's applications to allow for more accurate calculations if a conventional method such as modified Raoult's law is used.

Key words: Kuiper belt objects: individual: Pluto – planets and satellites: atmospheres

1 INTRODUCTION

Extreme conditions at low temperatures on extraterrestrial bodies introduce an important feature to their atmospheres, where all major chemical components in the atmosphere are condensable, thus participating in phase transitions and equilibria that may occur on the surface or at some altitudes from the surface. A well-known example is Titan's lower atmosphere, which is in vapour-liquid equilibrium (VLE) near and on the surface, not only to maintain the liquid phase in its lakes or seas, but also to produce the profile of atmospheric methane with altitude that was measured by Huygen's probe (Tan, Kargel & Marion 2013; Tan & Kargel 2018a). This is in contrast with our atmosphere on Earth that has high temperatures so that any phase transitions effectively do not involve the major components (nitrogen, oxygen, argon). Water, as a component that condenses and evaporates in the atmosphere, can consequently be treated separately from the rest of the atmosphere due to its much higher triple point than that of the major components. Based on this fact, the concept of partial pressure of water becomes important in atmospheric sciences. However, in atmospheres with condensable major components, applications of partial pressures may lead to inaccuracies even if the pressure is very low such as that on Pluto, where the simple Raoult's law has been a common choice for modeling.

The inaccuracies arise from the fact that the solid phase is not an ideal solution; the ideality is assumed to be true in Raoult's law. Therefore, modeling under such conditions must be able to account for phase equilibria that involve non-ideal solid solutions. Though the non-ideality can be fixed using the concept of activity coefficient, such as in the modified Raoult's law, the coefficients are not readily calculated (Trafton 2015). In this study, an equation of state (EOS) that has the required ability is applied: CRYOCHEM 2.0, which has been used for the vapour-solid equilibrium (VSE) on Pluto's surface (Tan & Kargel 2018b). Using this EOS, the activity coefficients can be calculated for those who still need to apply the modified Raoult's law.

This study is in fact an extension of that on the VSE at Pluto's surface (Tan & Kargel 2018b). Above the surface, the phase equilibria are subject to hydrostatic effects due to gravity that vary with altitudes. Therefore, by coupling CRYOCHEM with the hydrostatic effects and adopting a realistic temperature profile, the deposition point of the atmosphere can be located; it is the altitude above which solid phases can no longer exist in the atmosphere. In addition, the vertical profiles of pressure and density below the deposition point can be determined as well as the corresponding compositional profiles in the equilibrium phases. Note that the discussion in this study is merely based on thermodynamic equilibrium, where any implications leading to temporal variations and fluid dynamics in the atmosphere are not considered, thus open for further investigations. The results may serve as the limiting case from quasi-equilibrium conditions as done before for the VSE on Pluto's surface (Tan & Kargel 2018b).

2 PLUTO'S LOWER ATMOSPHERE

Pluto's atmosphere may be treated as a binary mixture of nitrogen and methane, N_2/CH_4, which is verified to be accurate enough for various applications including the phase equilibria with solid phases on the surface (Tan & Kargel 2018b). This is true partly due to the tiny amount of the third most abundant component (carbon monoxide), which also happens to have similar properties to the most dominant component (nitrogen). The atmospheric methane mixing ratio was derived from New Horizons solar UV occultation to be 0.6-0.84 per cent on the surface (Gladstone et al. 2016), but later superseded with 0.28-0.35 per cent (Young et al. 2018). Two compositions will be considered in this work for comparison purposes: 0.6 and 0.3 mole per cent of methane.

* email: stan@psi.edu

A realistic temperature profile of the lower atmosphere for this study is taken from Hinson et al. (2017) who derived the density, temperature, and pressure profiles based on radio occultation performed by New Horizons down to 1 km above the surface with an assumption of pure-nitrogen atmosphere. Only the condition for the case of ingress (sunset), at which the binary N_2/CH_4 can undergo phase equilibria, is discussed here. While the temperature profile is used as one of the inputs for the calculations in this study, the density and pressure profiles can be used for validation of the calculations. Therefore, the results in this study, which include the deposition point and the phase compositional profile below it, give a more complete picture of the lower atmosphere near the surface when the condition allows phase equilibria. The correlation of the temperature profile for computation purposes in this work is given in Appendix A.

At low temperatures, the lowest part of the atmosphere can be in equilibrium with solid phases. Therefore, the composition of the atmosphere becomes the overall composition that includes all the equilibrium phases, not just the vapour (gaseous part of the atmosphere). Due to the latent heat released at the deposition process, the situation is similar to that of a cloud in VLE with wet adiabat (Sanchez-Lavega 2011). In this situation, any instability of the atmospheric columns will cause vertical wet convection (Jacob & Prather 1990), thus maintaining a well-mixed condition with a constant overall composition independent of altitudes. Such phase equilibrium with well-mixed condition is present on Titan (Tan et al. 2013; Tan & Kargel 2018a) and expected to be valid on Pluto as well, but with solid phase instead of liquid. In this work, all calculations start at 1 km altitude, which is the lowest altitude where the atmospheric conditions were measured by Hinson et al. (2017), both downward to the surface and upward towards the deposition point at a higher altitude.

3 PHASE EQUILIBRIA

At low pressures, there is no doubt that ideal-gas assumptions are valid, which carry a lot of simplification in modeling to describe the properties of gas mixtures such as their densities and compositions. However, if the conditions are also at low temperatures where the solid phase may be present, such as that on Pluto, the advantage of the simple ideal-gas behavior may be offset by the complexity coming from the deposited solid solutions, as shown later.

The condensed phase diagram of N_2/CH_4 binary mixture, Fig. 1(a), is commonly used as a guide to determine whether the mixture is in liquid, solid, coexisting liquid/solid, or solid/solid phases. For our discussion on the atmosphere, the missing phase not shown in the figure is the vapour phase. In fact, this diagram can also be constructed without losing accuracies using data measured from a three-phase vapour-solid-liquid (VLS) and vapour-solid-solid (VSS) equilibria (Ricci 1951; Omar et al. 1962), which means that every point on the phase boundaries is also in equilibria with the vapour phase. Therefore, it may be concluded that the phase boundaries are under their own vapour pressures, as opposed to isobaric diagram at a constant pressure. The accuracy is not lost because condensed phases are insensitive to low and moderate pressures.

However, the use of the condensed phase diagram in Fig. 1(a) needs caution. For example, according to Fig. 1(a) at temperatures below 55 K, which is the temperature range of interest for Pluto's lower atmosphere in this work, the phase equilibrium is between solid solutions S_1 (nitrogen-rich solid) and S_2 (methane-rich solid), or in fact a three-phase equilibrium between vapour and those two solids (VS_1S_2). Therefore, for discussions in this study, the presence of vapour needs to be explicitly shown so that the situation is better illustrated using an isobaric phase diagram such as in Fig. 1(b), which is calculated at the surface pressure of 12.8 μbar (Hinson et al., 2017). The total composition of the atmosphere (0.3 or 0.6 mole per cent of methane; they are indistinguishable in the figure due to the scale) is represented by the filled circle at the surface temperature of 38.9 K, which lies inside the two-phase region of VS_2. In other words, the phase diagram indicates that the atmosphere on Pluto's surface is in VS_2E at 38.9 K and 12.8 μbar.

Thermodynamically, the two-phase VSE may be expressed as the equality of the fugacity (f) of the individual component i (1 = nitrogen; 2 = methane) in the equilibrium phases (V = vapour; S = solid):

$$\hat{f}_i^{\mathrm{V}}(T,P,\mathbf{y}) = \hat{f}_i^{\mathrm{S}}(T,P,\mathbf{x}^{\mathrm{S}}) \qquad i = 1, 2 \qquad (1)$$

where T is the absolute temperature, P is the equilibrium pressure, while $\mathbf{y} = \{y_i\}$ and $\mathbf{x} = \{x_i\}$ are the compositions in mole fractions in the equilibrium vapour and solid phase, respectively. The equality can be written in terms of fugacity coefficients (φ) or equivalently activity coefficients (γ) as:

$$y_i\hat{\varphi}_i^{\mathrm{V}}(T,P,\mathbf{y})P = x_i^{\mathrm{S}}\hat{\varphi}_i^{\mathrm{S}}(T,P,\mathbf{x}^{\mathrm{S}})P \qquad i = 1, 2 \qquad (2a)$$

or

$$y_i\hat{\varphi}_i^{\mathrm{V}}(T,P,\mathbf{y})P = x_i^{\mathrm{S}}\gamma_i^{\mathrm{S}}(\mathbf{x}^{\mathrm{S}},T,P)\,f_{0,i}^{\mathrm{S}}(T,P) \qquad i = 1, 2 \qquad (2b)$$

Note that the activity coefficients only apply to the condensed phase, in this case the solid S in equation (2b). The fugacity of pure components in the solid phase in equation (2b) may be approximated using (Smith, Van Ness & Abbott 2005):

$$f_{0,i}^{\mathrm{S}}(T,P) \approx \varphi_{0,i}^{\mathrm{VS}}(T)P_i^{\mathrm{VS}}(T)\exp\left(v_i^{\mathrm{S}}(T)\frac{P-P_i^{\mathrm{VS}}(T)}{RT}\right) \qquad i = 1, 2 \qquad (3)$$

where the factors in front of the exponential are the fugacity coefficient of pure component i and its pressure in solid/vapour saturation at T, respectively. In the exponential, R is the gas constant and v_i is the molar volume of the solid of pure component i at T.

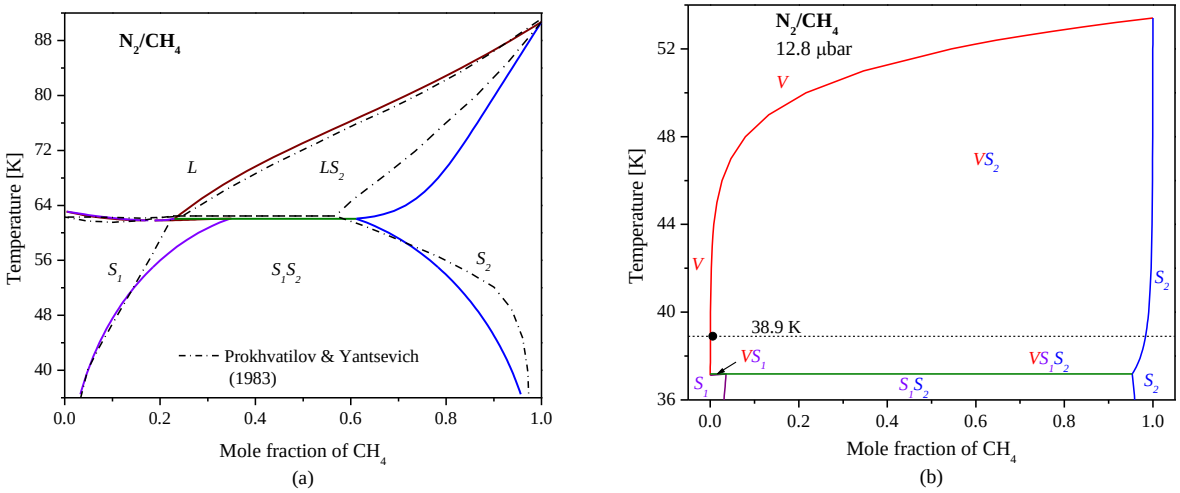

Fig. 1. Binary mixture of N_2/CH_4: (a) condensed phase diagram showing only condensed phases; (b) isobaric phase diagram at 12.8 μbar also showing the vapour phase. Solid curves are calculated using CRYOCHEM 2.0. The filled circle represents the total composition of 0.3 or 0.6 mole per cent of methane (indistinguishable here due to the scale – see Fig. 3a for clarity) at the surface condition of 38.9 K and 12.8 μbar; it is in the VS_2 region.

As mentioned earlier, the condition at low pressures validates the ideal-gas assumption for the vapour so that the fugacity coefficient in vapour in equation (2b) is unity. Furthermore, if the equilibrium pressure P is not much different from the saturation pressure P^{VS} of the individual components, or both pressures are equally low, the exponential in equation (3) is also close to unity. Applying these conditions, which are justifiable for Pluto, to equations (2b) and (3) leads to the so-called modified Raoult's law:

$$y_i P = x_i^S \gamma_i^S(\mathbf{x}^S, T, P) P_i^{VS}(T) \qquad i = 1, 2 \qquad (4)$$

The left-hand side of equation (4) is the partial pressure of component i in the vapour. If the activity coefficients of both components may be assumed to be unity, which means that the solid phase is an ideal solution, equation (4) is reduced further to the original Raoult's law, which can be expressed as:

$$x_i^S = \frac{y_i P}{P_i^{VS}(T)} \qquad i = 1, 2 \qquad (5)$$

Equation (5) means that the mole fraction of component i in solid phase is the ratio of its partial pressure in the vapour to its saturation pressure. Considering that the mole fraction is equal or less than unity, the equilibrium only occurs at conditions where the partial pressure is less than or equal to the saturation pressure. If those pressures are equal, the solid consists of pure component i.

However, the solid phases on Pluto are not ideal solutions (Cruikshank et al. 2015; Tan & Kargel 2018b), so that equation (5) is not accurate. Even with the modified Raoult's law, the non-ideality introduces difficulties because the right-hand side of equation (4) cannot be calculated due to the unknown activity coefficients (Trafton 2015). The non-ideality is discussed in Appendix B.

Therefore, the more general equation (2a) needs to be used by applying an EOS that can calculate fugacity coefficients in solid phases. As mentioned earlier in the introduction, CRYOCHEM 2.0 is such an EOS suitable for this work. The details and the performance of the EOS, as well as the parameters, may be reviewed in the previous paper (Tan & Kargel 2018b). The EOS can also calculate the activity coefficients for the modified Raoult's law, equation (4), the values of which are included in Appendix B.

All solid curves in Figs. 1(a) and (b) are calculated using this EOS. In Fig. 1(a), the calculated solid-phase boundaries are compared with the approximation from X-ray diffraction experiments (Prokhvatilov & Yantsevich 1983), which show consistency in describing the solid-solid region at temperatures below 55 K as used in Fig. 1(b) with some deviation mainly on the methane-rich side.

Equation (2a) consists of two independent equations coming from two components and two phases. Therefore, according to the phase rule, the equilibrium has a degree of freedom (DOF) of 2, which means that it may be determined if two independent variables are fixed, for example, the temperature T and pressure P, where the two equations in equation (2a) will then solve for two variables y_1^V and x_1^S, which are the equilibrium phase compositions. The mole fractions of the second component are calculated from the fact that the mole fractions in a phase sum to unity.

At even lower temperatures, three-phase VSS equilibrium may also occur. In this case, another equation representing the third phase must be added to equations (2a) and (2b) (see Tan & Kargel 2018b). According to the phase rule, the VSS equilibrium for a binary mixture has a DOF of 1, thus univariant similar to VS sublimation for pure gases, in which the saturated vapour pressure is just a function of temperature.

4 GRAVITATIONAL EFFECTS

As indicated in Fig. 1(b), the atmosphere near the surface is in VSE where the well-mixed condition requires the overall composition to be constant with altitudes. Above the surface, the equation of the hydrostatic pressure must be explicitly applied to be coupled with equation (2a):

$$dP = -\left(\frac{1-\sigma}{\rho^{\mathrm{V}}} + \frac{\sigma}{\rho^{\mathrm{S}}}\right)^{-1}\left((1-\sigma)\sum_i x_i^{\mathrm{S}} M_i + \sigma\sum_i y_i M_i\right) g(h)dh \tag{6}$$

where ρ^{V} and ρ^{S} are the molar densities of vapour and solid in the VSE at an altitude of h, respectively, while σ is the corresponding mole fraction of the solid phase that can be calculated from material balance:

$$y_i(1-\sigma) + x_i^{\mathrm{S}}\sigma = z_i \tag{7}$$

where $\mathbf{z} = \{z_i\}$ is the overall composition of the atmosphere. The compositions of the equilibrium phases $\mathbf{x}$ and $\mathbf{y}$ are obtained from solving equation (2a). For binary mixtures, equation (7) is needed only with $i = 1$ or 2 to solve for σ and commonly known as the lever rule.

The expression in the first parentheses in equation (6) calculates the total molar density and that in the second parentheses calculates the average of molar mass. The coupling of equation (6) and equation (2a) is carried out by applying them alternately as the altitude changes by increments of dh. The coupling stops at the deposition point where the mixture is about to exit the VSE.

In equation (6), Pluto's gravity may be written as a function of altitude h:

$$g(h) = g_0\left(\frac{1187.4}{R+h}\right)^2 \tag{8}$$

with R is Pluto's radius (1187.4 km for the ingress case – according to Hinson et al. 2017). The factor g_0 is the gravity on the surface (0.62 m/s^2 – Gladstone et al. 2016) assigned at the radius, which is close the global mean radius of 1188.3 ± 1.6 km (Nimmo et al. 2017).

4 RESULTS AND DISCUSSION

4.1 Phase diagrams

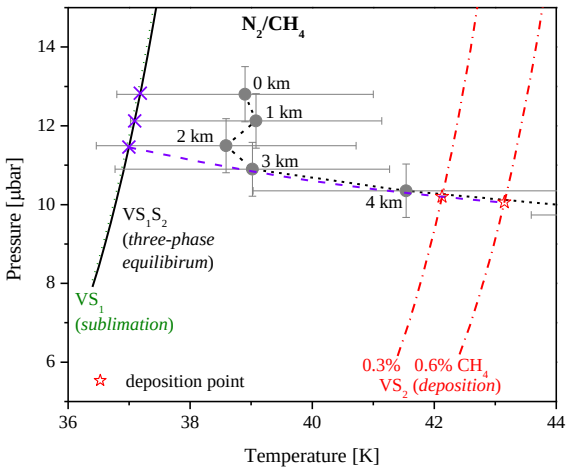

Fig. 2. Pressure-temperature profile of Pluto's lower atmosphere (at ingress of Hinson et al. 2017) and phase boundaries of binary N_2/CH_4 calculated using CRYOCHEM 2.0; the profile is represented by five lowest data points (at the altitudes of 0-4 km) along with their standard of deviation. The dotted curve connecting the data points is just a guide to the eye. For Scenario 2 (dashed curve – see text), the lowest three points are the crosses on the VSS curve.

As shown in Fig. 2, the pressure-temperature (*PT*) profile of the atmosphere at ingress of Hinson et al. (2017) intersects the calculated two-phase VS_2 boundary of the binary N_2/CH_4 at the deposition point, which is at the altitude of 4.26 km (42.13 K) for

0.3 mole per cent of methane and 4.54 km (43.15K) for 0.6 mole per cent of methane. Therefore, the atmosphere between the surface up to the deposition point is in VSE, where the solid phase is methane-rich solid (S_2) as identified earlier in Fig. 1(b).

It is also clear in Fig. 2 that the *PT* profile of Pluto's lower atmosphere is above the three-phase VS_1S_2 curve of binary N_2/CH_4, which happens to be very close to the two-phase VS_1 boundary of the binary (the difference between cases of 0.3 and 0.6 mole per cent of methane is not observable on the diagram) as well as the sublimation curve of pure nitrogen (not shown in the figure for clarity). Fig. 3(a) magnifies the part of Fig. 1(b) in the vicinity of three-phase temperature and VS_1. At 12.8 μbar in Fig. 3(a), the temperatures of VS_1S_2, VS_1 boundary (stars), and sublimation point of N_2 (point F) are calculated to be very close to one another: 37.18 K, 37.14 K (0.6 mole per cent of methane), and 37.13 K, respectively.

Therefore, if the atmosphere were pure nitrogen, it would not undergo deposition in the given temperature profile, unless the errors of temperature are included. As seen in Fig. 2, the error bars of the lowest 4 data points overlap with the VSS, VS_1, and pure nitrogen sublimation curves. For example, on the surface at 12.8 μbar, the standard deviation is ±2.1 K (Hinson et al. 2017) so that the lower bound is 36.8 K, thus below the deposition point of pure nitrogen (37.13 K) and the three-phase VSS temperature of the binary (37.18 K), as well as the VS_1E of the binary, which occurs between those temperatures. In this case, the mixture must go across the three-phase temperature as one descends to the surface. More about this will be discussed later.

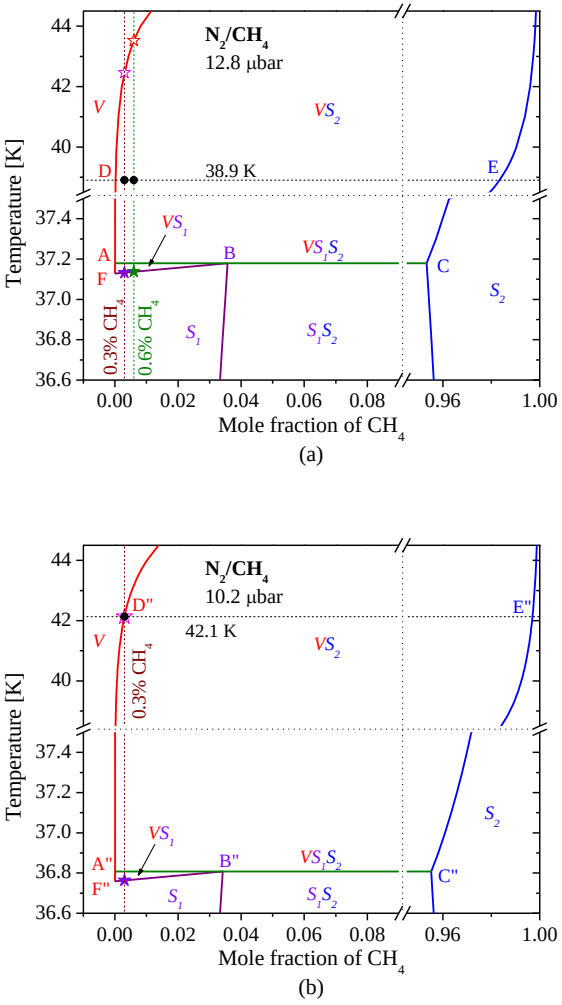

Fig. 3. Isobaric phase diagrams: (a) at 12.8 μbar, circles at 38.9 K represent the conditions on the surface for 0.3 and 0.6 mole per cent of methane; (b) at 10.2 μbar, which is the pressure at the deposition point for 0.3 mole per cent of methane (42.1 K). Filled stars are sublimation points and empty stars are deposition points at the respective pressures. Points A, B, and C, as well as A″, B″, and C″ are VSSE compositions, while points D, E, D″ and E″ are VS_2E compositions. F and F″ are the sublimation of pure nitrogen. Dotted lines are breaks.

Figs. 3(a) and 3(b) are isobaric phase diagrams at 12.8 μbar and 10.2 μbar, which are the pressures at the surface and at the altitude of 4.26 km (the deposition point of the mixture with 0.3 mole per cent of methane), respectively. Despite the different pressures, the phase diagrams look similar to each other with the latter shifted by less than 0.4 K to lower temperatures as seen by comparing the three-phase temperatures, which are lines ABC in Fig. 3(a) and A″B″C″ in Fig. 3(b). Coincidentally, the lower

pressure is also the pressure on the surface for the egress (sunrise) case in Hinson et al. (2017), so that Fig. 3(b) can also be used to evaluate the phase of the atmosphere at the egress condition. Because the corresponding temperature on the surface is 51.6 K (Hinson et al. 2017), which is way above the VS_2 region for both evaluated total compositions, the atmosphere is in the homogeneous vapour phase, thus no solid is present.

Figs. 3(a) and 3(b) also provide the conditions of VSE on the surface and deposition point, respectively, plotted as black circles at the respective temperatures of 38.9 K and 42.1 K. The equilibrium compositions at the VS_2E are given by points D and E at 38.9 K, and D″ and E″ at 42.1 K. The mixture properties at all points are given in Appendix C. Note that D″ is the same as the deposition point for 0.3 mole per cent of methane at the altitude of 4.26 km, while D and E serve as the equilibrium composition for both total compositions with 0.3 and 0.6 mole per cent of methane. At the VSS temperatures, A and A″ are equilibrium compositions in vapour, B and B″ in nitrogen-rich solid S_1, and C and C″ in methane-rich solid S_2.

In the VS_2E of Pluto's atmosphere below the deposition point, the solid phase is methane rich. To find the nitrogen-rich solid (S_1), one needs to cool the mixture down across the VSS temperature entering the two-phase VS_1 region (small triangular region ABF in Fig. 3a). In this VS_1E, the vapour is in equilibrium with solid S_1. At the surface pressure of 12.8 μbar, the sublimation points (filled stars) are at 37.13 K for 0.3 mole per cent of methane and 37.14 K for 0.6 mole per cent of methane, right below the three-phase VSS temperature of 37.18 K. Thus, only within this 0.04-0.05 K range can the nitrogen-rich solid exist at this pressure in the presence of vapour.

None the less, as mentioned above, the isobaric phase boundaries shift down to lower temperatures when the pressure changes from 12.8 to 10.2 μbar. Therefore, as the pressure of the atmosphere drops upon cooling, or increases upon heating, the VS_1 equilibrium may live longer as it also shifts with the temperature change. Since VS_1 must occur below the three-phase VSS temperature, sublimation from S_1 to VS_1 upon heating must occur before the VSS temperature, and upon cooling, the disappearance of S_2 replaced by S_1 must first occur at the VSS temperature. For any total compositions smaller than point B at the VSS temperature in Fig. 3(a), S_1 and S_2 are in equilibrium with vapour, with S_1 being transformed into S_2 upon heating and the reverse upon cooling. The system stays at the equilibrium following the VSS curve (such as in Fig. 2) until one of the equilibrium solid phases is completely transformed before proceeding to the two-phase equilibrium with the other solid. In an open atmosphere with an established pressure like Earth's, the temperature remains constant during the phase transformation.

Since S_1 and S_2 are both observed on Pluto surface, with S_1 in colder region and S_2 in warmer region consistent with the phase diagram, there are two possible scenarios for the fate of the solid phases upon heating/cooling in equilibrium with the atmosphere, named as Scenario 1 and Scenario 2 in this study. We will use isobaric phase diagrams such as that in Fig. 3 to illustrate the scenarios. Even though the diagrams individually cannot describe the dynamics of sublimation and deposition processes, they can serve as snapshots at different pressures as the temperature change is in progress. While the hydrostatic pressure changes with altitude, the temperature also changes due to the existing gradient, so a series of isobaric phase diagrams are needed to illustrate the progression as one moves vertically in the atmosphere.

In Scenario 1, the solids S_1 and S_2 can individually exist without the presence of the other, so that S_2 must exist above the VSS temperature and S_1 must exist below it. As an illustration, S_2 can eventually change completely to S_1 through cooling as follows. Starting from a high temperature with no solid, solid S_2 appears upon cooling after the temperature crosses the deposition point (isobarically the empty stars in Figs. 3a-b) thus entering VS_2 region. Further cooling will eventually put the system at VSS, where the first chunk of solid S_1 appears. Based on the calculated properties in Appendix C for the condition in Fig. 3(a) and 0.3 mole per cent of total methane, the lever rule gives the mole fraction of S_2 to be 0.31 per cent when the mixture arrives at VSS. This is when the transformation from S_2 to S_1 begins as the cooling proceeds while releasing heat. As S_2 disappears, S_1 grows from 0 to 8.27 mole per cent when the transformation is completed, which indicates that some vapour also deposits into S_1 in the process, thus reducing the pressure. This means that the transformation proceeds along the VSS curve. The calculation using the lever rule is also included in Appendix C.

After the transformation is completed, further cooling will lower the temperature and pressure in two-phase VS_1 equilibrium while more vapour deposits into S_1. Since the temperature and pressure both drop in the cooling process, the sublimation point may not be reachable as it is implied from current models that the atmosphere never collapses (Olkin et al. 2015; Sicardy et al. 2021). Upon heating, this scenario is reversed. When the mixture arrives at VSS from VS_1, the mole fraction of S_1 is 8.27 per cent. As the heating continues, some of S_1 transforms into S_2, which grows from 0 to 0.31 mole per cent when the transformation is completed, thus most of it evaporates and increases the pressure. This is how the atmospheric pressure grows along the VSS curve.

Based on the current known conditions, S_2 can exist by itself, e.g. as observed in the massive methane deposits on bladed terrain of Tartarus Dorsa (Moore et al. 2018). In the event of supercooled atmosphere or that with finely dispersed solid S_2, the blade-like ridges in the terrain may get the deposit solid directly from the atmosphere, just like frost induced on solid surfaces soaked in supercooled vapour. This process is different from that proposed by Bertrand et al. (2020), in which vertical transport of gaseous methane is needed for deposition at higher elevation. However, if the vertical convection maintaining the well-mixed condition is considered, then both processes may be in line with each other.

In colder regions such as Sputnik Planitia, S_1 may exist by itself indicating temperatures below that of VSS. Consequently, there must be transitional regions or altitudes at VSS temperatures, where solid S_1 and S_2 are in equilibrium at the vapour pressure of the mixture. Indeed, both solids can coexist at low elevations (Moore et al. 2018). In Scenario 2, the lowest part of the atmosphere

is stuck in VSS equilibrium, where the solids S_1 and S_2 coexist by any proportions, while the residual vapour maintains a tenuous atmosphere at low pressures. The proportion of S_1 and S_2 within the solid phases can be of any values depending on the net released heat upon cooling or the net heat received upon heating. For the latter, only if the heat is enough to transform all S_1 into S_2 and some vapour, can the system proceed to VS_2 as discussed in the first scenario. Quantification based on the released or required heat is beyond the current study thus open to future investigations. Therefore, for the calculations here, it is assumed that solid S_1 is the incipient phase so that the density ρ^S, composition $\mathbf{x}^S$, and solid mole fraction σ used in equations (6) and (7) all belong to S_2. This assumption is safe to use due to the much smaller mole fractions of S_1 and S_2 than that of vapour (Appendix C).

If further drop from the VSS temperature is allowed, the system may eventually reach the four-phase equilibrium with the appearance of an additional solid phase of nitrogen (α phase) near its transition point at 35.4 K and 4.84 bar (Frels, Smith & Ashworth 1974). In this case, the binary N_2/CH_4 will be also stuck at the invariant four-phase equilibrium until all S_1 is completely transformed into S_1^{α}, which is solid rich with α nitrogen. We will not discuss this four-phase equilibrium in this study.

4.2 Vertical profiles

With the temperature profile in Appendix A as input for the calculations, the resulting pressure and density profiles up to the deposition point for Scenario 1 are presented in Fig. 4(a), which agree well with the data derived from radio occultation (Hinson et al., 2017) that treated the atmosphere to consist of nitrogen only. This proves that the minor component, methane, is insignificant in the data derivation. However, pure-nitrogen atmosphere may not undergo any phase transitions at the measured conditions (unless the error of temperature is included as discussed earlier), while the binary mixture of N_2/CH_4 does.

As mentioned earlier, for the VS_2E at altitudes below the deposition points, the atmosphere is well mixed with a constant total composition (0.3 or 0.6 mole per cent of methane). The resulting compositional profiles in the equilibrium vapour and solid phase are represented by the mole fractions of methane and nitrogen, respectively, as shown in Fig. 3(b). Note that in VS_2E, the total compositions of 0.3 and 0.6 mole per cent of methane give the same profiles up to their respective deposition points. Methane mostly stays in solid phase in the lowest 3 km while the solid-phase mole fraction is close to that of the total methane mole fractions. The minimum mole fraction of methane in vapour is 1.85×10^{-2} per cent at the altitude of 2 km, where the mole fraction of nitrogen in the S_2 solid reaches the maximum at 1.76 per cent. All calculated profiles in this work are given in the supplementary material that accompanies the paper.

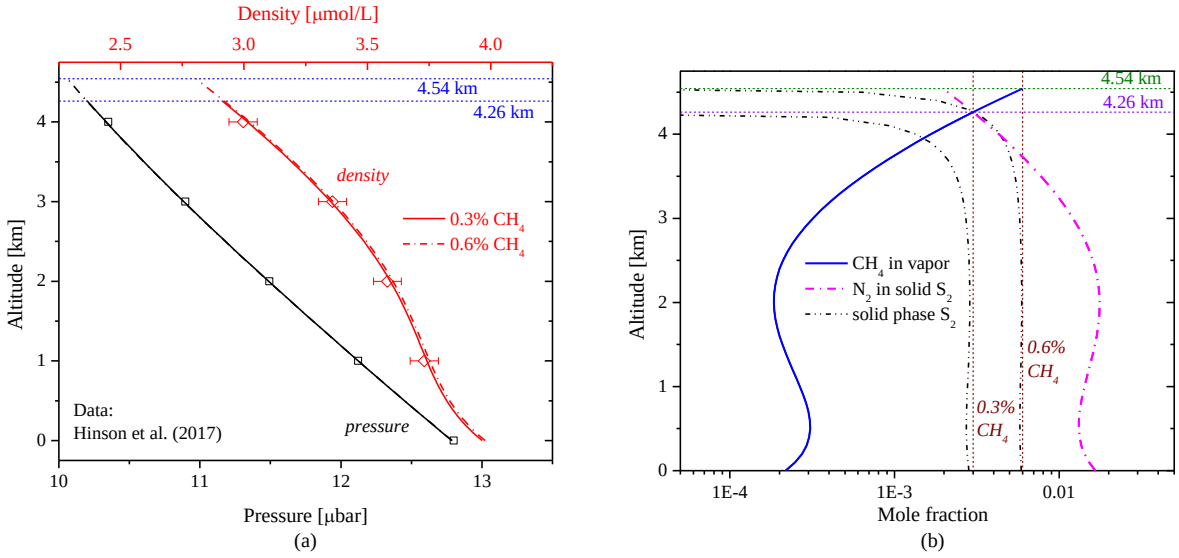

Fig. 4. (a) Pressure and density profiles of Pluto's lower atmosphere: data from radio occultation (Hinson et al., 2017) and curves from VS_2E calculations for Scenario 1. Deposition points are at 4.26 km and 4.54 km (for 0.3 and 0.6 mole per cent of methane, respectively); (b) the corresponding compositional profiles below the deposition points.

It has been recognized that the gaseous mixing ratio of methane near the surface is way more than the mole fraction needed at equilibrium, which is less than 0.032 mole per cent below the altitude of 3 km (Fig. 4b), which is about 10 times lower than the currently accepted mole fraction of 0.3 per cent (Gladstone & Young et al. 2019). A possible explanation is that, in the VSE, the mixing ratio is to be associated with the overall mole fraction of methane, which is constant with altitudes due to well-mixed condition up to the deposition point (the vertical dotted lines at 0.3 or 0.6 mole per cent in Figs. 4a-b). The total methane mole fraction of 0.3 per cent is favorable here due to the lower deposition point at 4.26 km, which is closer to the estimated altitude of the top of surface boundary layer – 4 km (Gladstone & Young 2019), thus consistent with the mixing ratio estimated by extrapolation from solar occultation (Young et al. 2018).

For Scenario 2, the lower atmosphere is under its own vapor pressure along the VSS curve of the binary N_2/CH_4. This may happen, for example, if the lowest three points in Fig. 2 are shifted to the VSS curve, thus near the lower bounds of their original temperature data. This hypothetical *PT* profile is still allowed within the errors shown in Fig. 2. The original pressure at the altitude of 1 km is maintained to be 12.123 μbar (Hinson et al. 2017). While the temperature is determined to be along the VSS curve, the pressure follows the hydrostatic equation (6). It is also assumed that the atmosphere leaves the VSS curve at the altitude of 2 km such that a smooth *PT* curve may be obtained downward from the VS_2 region in Fig. 2 (dashed curve). For computation, the correlation of temperature profile above 2 km throughout the VSE is given in Appendix A.

As shown in Fig. 5(a), the calculated densities do not match with the data from Hinson et al. (2017). Therefore, the hypothetical Scenario 2 did not happen, but Scenario 1 as observed by New Horizons. However, it may occur sometime later, at least qualitatively, when the temperature declines as Pluto is receding from the Sun. While the pressure profile stays smooth, those of phase compositions do not. The compositions have abrupt changes of slope at 2 km as the phase equilibrium changes from VSE to three-phase VSS downward to the surface.

5 CONCLUSIONS AND REMARK

When the temperature is low enough, such as that in ingress case of radio-occultation data (Hinson et al. 2017), Pluto's lower atmosphere undergoes two-phase VSE, in which the solid is methane rich (S_2). This phase equilibrium is not limited to the surface but also upward to the deposition point, above which the atmosphere is in gaseous phase. For a higher total mole fraction of methane in the atmosphere, the deposition point is at a higher elevation. Therefore, the location of the deposition point can give us a clue about the overall composition of the atmosphere at and below the point.

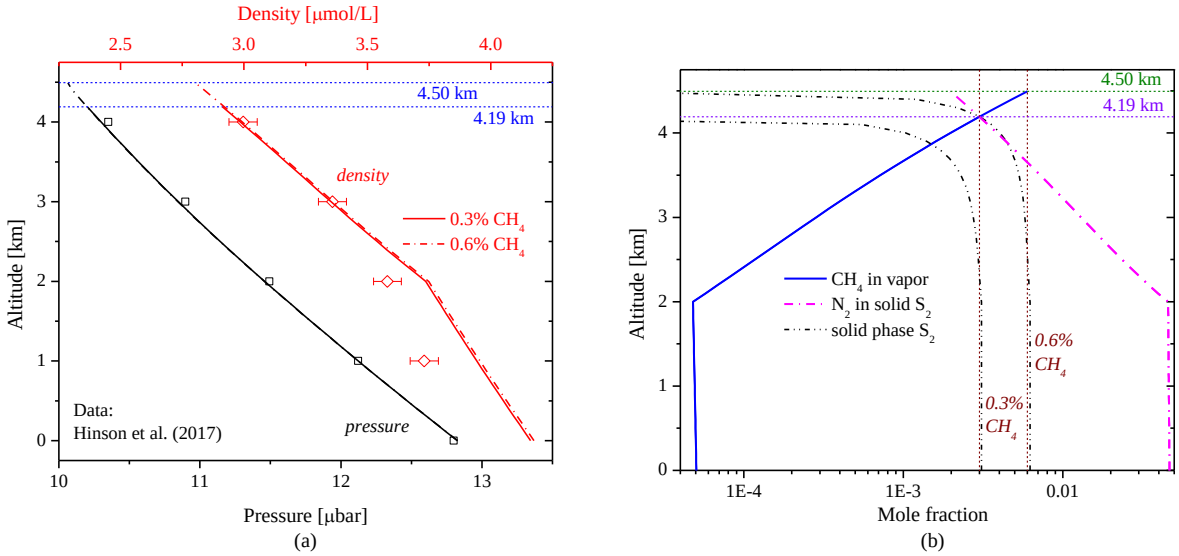

Fig. 5. (a) Pressure and density profiles of Pluto's lower atmosphere: data from radio occultation (Hinson et al., 2017) and curves from Scenario 2: VSSE and VS_2E calculations below and above 2 km, respectively. Deposition points are at 4.19 km and 4.50 km (for 0.3 and 0.6 mole per cent of methane, respectively); (b) The corresponding compositional profiles below the deposition points.

The location of the deposition point at an altitude of about 4 km is comparable with the top of distinct boundary layer where the temperature inversion ends at ingress case as observed in radio occultation (Hinson et al. 2017; Gladstone & Young 2019). It means that the atmosphere is in two-phase VS_2 equilibrium within the boundary layer down to the surface as described in Scenario 1 in this study. As mentioned earlier, the situation is like inside a cloud with wet adiabat, where any instable atmospheric columns induce vertical wet convection, thus maintaining constant overall composition independent of altitude towards the well-mixed condition.

If the lower atmosphere is correctly assumed to be in vapor-pressure equilibrium on the surface, then it must be in equilibrium with two solid phases S_1 and S_2, i.e. VSS as discussed in Scenario 2 in this study. Even though the scenario was not observed by New Horizons, as evident from the mismatch of calculated density with the data in Fig. 5(a), it may occur at a lower temperature profile when Pluto is far enough from the Sun. As shown in Fig. 2, the VSS curve is very steep in pressure, so that the appearance of S_1 is more likely due to the lowering of temperature rather than the increase of pressure. The latter was previously proposed for the abundance of S_1 in Sputnik Planitia; it is associated with the higher pressure due to lower altitude that leads to a higher deposition temperature (Bertrand & Forget 2016).

Though the relation between the boundary layer and vapour-solid phase equilibria still needs further investigation, the presence of multiple phases in the layer will introduce a new environment to consider in modeling, which may further provide new insights for better understanding. For those who still need to apply the modified Raoult's law in their modeling, more accurate calculations are possible by applying equation (4) and the activity coefficients given in Appendix B.

ACKNOWLEDGEMENTS

This work was supported by NASA Solar System Workings Grant # 80NSSC19K0792.

DATA AVAILIBILITY

The data resulting from calculations in this article are available in the article and in its online supplementary material.

REFERENCES

Bertrand T., Forget F., 2016, Nature, 540, 86
Bertrand T. et al., 2020, Nat. Commun., 2020, 11, 5056
Cruikshank D. P. et al., 2015, Icarus, 246, 82
Frels W., Smith D.R., Ashworth T., 1974, Cryogenics, 14, 3
Gladstone G. R. et al., 2016, Science, 351, 1280
Gladstone G.R., Young, L.A., 2019, Annu. Rev. Earth Planet. Sci., 47, 119
Hinson D.P. et al., 2017, Icarus, 290, 96
Jacob D.J., Prather M.J., 1990, Tellus, 42B, 118
Moore J.M. et al., 2018, Icarus, 300, 129
Nimmo F. et al., 2017, Icarus, 287, 12
Olkin C.B. et al., 2015, Icarus, 246, 220
Omar M.H. et al., 1962, Physica, 28, 309
Prokhvatilov A. L., Yantsevich L. D., 1983, Sov. J. Low Temp. Phys., 9, 94.
Ricci J.E., 1951, The Phase Rule and Heterogeneous Equilibrium. D. Van Nostrand Company, Inc., New York
Sanchez-Lavega, A, 2011, An Introduction to Planetary Atmospheres. Taylor & Francis, Boca Raton, FL
Sicardy, B. et al., 2021, ApJL, 923, L31
Smith J.M., Van Ness, H.C., Abbott, M.M., 2005, Introduction to Chemical Engineering Thermodynamics, 7th ed. McGraw-Hill, New York
Tan S. P., Kargel, J. S., Marion, G. M., 2013, Icarus, 222, 53
Tan S. P., Kargel J. S., 2018a, Fluid Phase Equilib., 458, 153
Tan S. P., Kargel J. S., 2018b, MNRAS, 474, 4254
Trafton L. M., 2015, Icarus, 246, 197
Young L. A. et al., 2018, Icarus, 300, 174

APPENDIX A: TEMPERATURE PROFILE

The temperature profile is taken from the ingress (sunset) case of Hinson et al. (2017). In this work, the following correlation up to the altitude of 5.6 km is made to match the data at the lowest altitude of 1 km (T_1 = 39.08 K) and then used as input for calculating the pressure/density and composition profiles with 1-meter altitude increments through the coupling of equations (2a) and (6).

$$T(h) = T_1 + \sum_{i=1}^{6} a_i (h-1)^i \qquad \text{[K]; } h \text{ in [km]} \qquad \text{(A1)}$$

where the coefficients a_1 = -0.67478, a_2 = -0.213172, a_3 = 0.487843, a_4 = -0.135041, a_5 = 0.019251, and a_6 = -1.025701 × 10^{-3}.

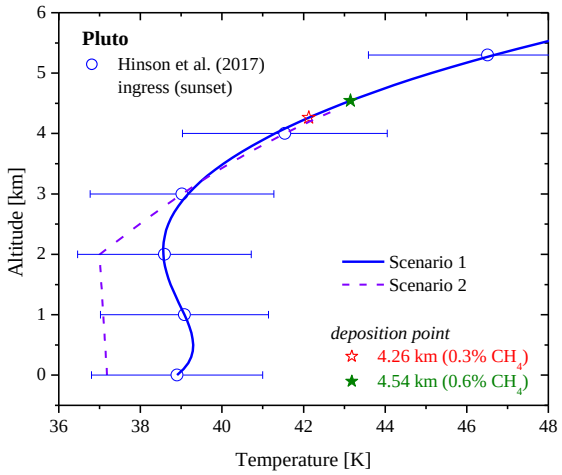

Fig. A1. Temperature profile from Hinson et al. (2017) and its correlations given by equation (A1) for Scenario 1 and equation (A2) for Scenario 2.

Equation (A1) is used for Scenario 1, which has VSE down to the surface, but for Scenario 2, the VSE is assumed to be only down to the altitude of 2 km with the following correlation for the temperature profile:

$$T(h) = \sum_{i=0}^{3} a_i h^i \tag{A2}$$

with the coefficients a_0 = 32.13321, a_1 = 3.283042, a_2 = -0.618085, a_3 = 0.096312. It is plotted on Fig. A1 as the dashed curve with nearly vertical slope below 2 km, where the temperature profile follows the VSS curve. The corresponding *PT* diagram is given in Fig. 2.

APPENDIX B: NON-IDEALITY

From equations 2(a) and 2(b), the activity coefficients in the solid phase can be expressed in terms of fugacity coefficients and calculated using EOS:

$$\gamma_i^{\mathrm{S}}(\mathbf{x}^{\mathrm{S}}, T, P) = \frac{\hat{\varphi}_i^{\mathrm{S}}(T, P, \mathbf{x}^{\mathrm{S}})}{\varphi_{0,i}^{\mathrm{S}}(T, P)} \tag{A3}$$

Both fugacity coefficient and activity coefficient are the measure of non-ideality, with the former relative to ideal gas and the latter relative to ideal solution. Large deviations from unity indicate severe non-ideality. For example, in the VS_2 range of the atmosphere below the deposition point, the activity coefficients in S_2 are plotted against altitude in Fig. A2(a), which shows that only the activity coefficient of methane is close to unity so that Raoult's law (equation 5) is valid for it. This is true because S_2 is a methane-rich solid, thus close to pure methane. On the other hand, the activity coefficient of nitrogen in S_2 is extremely large because nitrogen molecules cannot stay in an ideal solution with the methane majority as they have different crystalline structures, which are hexagonal versus cubic, respectively.

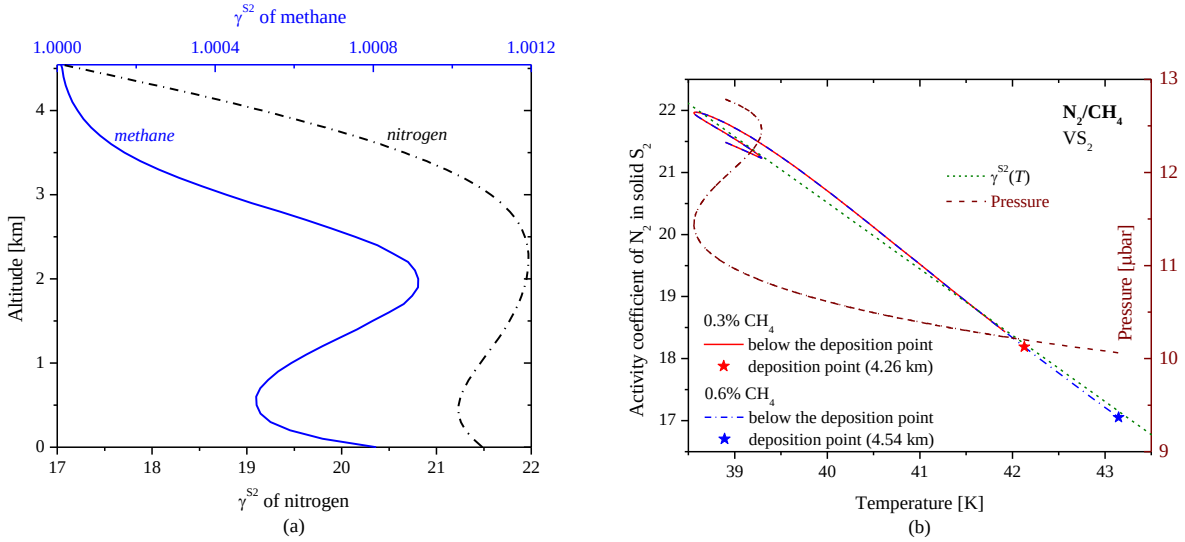

Fig. A2. The activity coefficients in S_2 (methane-rich solid) at VSE: (a) of nitrogen and methane plotted against altitudes; (b) of nitrogen plotted against temperature along with the linear correlation and the corresponding hydrostatic pressure in two-phase VS_2 equilibrium. The curves for cases of 0.3 and 0.6 mole per cent of methane are indistinguishable except for their different deposition points.

If the activity coefficient of nitrogen in S_2 is plotted against temperature, as shown in Fig. A2(b), it is almost linearly dependent on temperature with weak dependence on the pressure. It can be safely correlated as a linear function with an overall relative error of only 0.43 per cent for the lower atmosphere under the deposition point:

$$\gamma_{N2}^{S2}(T) = 63.21385 - 1.06755\ T \tag{A4}$$

This function can be used for both mole fractions of 0.3 and 0.6 mole per cent of methane, or any smaller compositions.

In VS_1 equilibrium, the opposite is true, where the activity coefficient of nitrogen in S_1 is almost unity because S_1 is a nitrogen-rich solid while the coefficient of methane in S_1 is much larger due to the non-ideality of methane molecules in the nitrogen-rich solid. Since this VS_1 is a very narrow region close to the VSS, the activity coefficient of methane in S_1 can be demonstrated in the three-phase VS_1S_2 equilibrium together with that of nitrogen in S_2 in Fig. A3.

The activity coefficients are under the vapour pressure of the binary mixture along the VSS curve and can be correlated with functions of temperature only in the temperature range of 35.4 – 45 K shown in Fig. A3 as follow:

$$\gamma_{N2}^{S2}(T) = 656.0907 - 40.4113\ T + 0.8585\ T^2 - 6.2184 \times 10^{-3} T^3 \tag{A5a}$$

$$\gamma_{CH4}^{S1}(T) = 960.1849 - 59.7989\ T + 1.2795\ T^2 - 9.3146 \times 10^{-3} T^3 \tag{A5b}$$

These two activity coefficients were estimated in Trafton's paper (2015) using their ratios to the activity coefficients of nitrogen in S_1 and methane in S_2, respectively, both of which are nearly unity as discussed earlier. Because the ratios were then derived graphically from the solid-phase boundaries on the condensed phase diagram proposed by Prokhvatilov & Yantsevich (1983) shown in Fig. 1a, any difference seen in Fig. A3 merely reflects the discrepancy between the phase boundaries calculated using CRYOCHEM and those estimated by Prokhvatilov & Yantsevich (1983).

Note that equations (A4) and (A5a) both describe the activity coefficient of nitrogen in S_2, but in different phase equilibria, VS for the former and VSS for the latter.

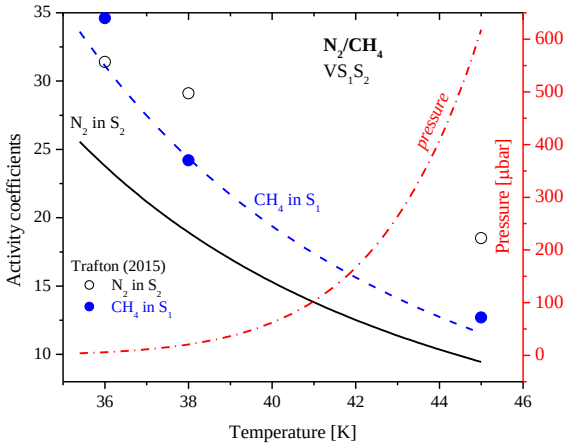

Fig. A3. The activity coefficients of nitrogen in methane-rich solid S_2 and methane in nitrogen-rich solid S_1 when the binary mixture is in three-phase VS_1S_2 equilibrium. Estimation by Trafton (2015) is also shown as circles in the figure.

APPENDIX C: PROPERTIES OF N_2/CH_4 AT POINTS ON FIGS. 3(a-b)

The pressure, temperature, phase type, composition, and density of binary N_2/CH_4 at equilibrium points A-E on Fig. 3(a) and points A″-E″ on Fig. 3(b) are listed in Table A1.

Below are examples in the text on the lever rule for Fig. 3(a) using equation (7) and the data in Table A.1 at 12.8 μbar.

Upon cooling, the mixture with 0.3 mole per cent of CH_4 arrives at the VS_1S_2 temperature from VS_2 region between point A (vapour) and C (solid S_2), so that the mole fraction of solid S_2 is:

$$\sigma_{S2} = \frac{0.3 - A}{C - A} = \frac{0.3 - 5.04 \times 10^{-3}}{95.33 - 5.04 \times 10^{-3}} = 0.31 \quad \text{mole \%} \qquad \text{(A6a)}$$

After the transformation of S_2 to S_1 is completed, the lever rule is applied between point A (vapour) and point B (solid S_1):

$$\sigma_{S1} = \frac{0.3 - A}{B - A} = \frac{0.3 - 5.04 \times 10^{-3}}{3.57 - 5.04 \times 10^{-3}} = 8.27 \quad \text{mole \%} \qquad \text{(A6b)}$$

The balance of these solid mole fractions is the vapour phase, so that equations (A6a) and (A6b) indicate a reduction of 8.27 – 0.31 = 7.96 mole per cent of vapour phase during the cooling across the three-phase VS_1S_2 temperature. In other words, the transformation of S_2 to S_1 is accompanied by the deposition of that much vapour into S_1.

Table A1. Properties of N_2/CH_4 at points on Figs. 3(a-b)

Point	T [K]	Phase	Mole% CH_4	Density [mol/L]
		P = 12.8 μbar (Fig. 3a)		
A		V	5.04×10^{-3}	4.14×10^{-6}
B	37.2	S_1	3.57	35.43
C		S_2	95.33	33.05
D	38.9	V	0.022	3.96×10^{-6}
E		S_2	98.34	32.91
		P = 10.2 μbar (Fig. 3b)		
A″		V	4.56×10^{-3}	3.33×10^{-6}
B″	36.8	S_1	3.42	35.46
C″		S_2	95.52	33.06
D″	42.1	V	0.30	2.91×10^{-6}
E″		S_2	99.70	32.74

DOI: 10.1093/mnras/stac1884

Supplementary Material

Low-pressure and low-temperature phase equilibria applied to Pluto's lower atmosphere

Sugata P. Tan
Planetary Science Institute

Figure 1b

Isobaric at 12.8 μbar

These data are also used for Fig. 3a

VS2

	vapor	*solid S2*	
T [K]	*yCH4*	*xCH4*	
37.1797	**0.00005041**	**0.95330248**	**VS1S2**
37.3	0.00005615	0.95712516	
37.5	0.00006705	0.96255627	
37.7	0.00007987	0.96708091	
37.9	0.00009492	0.97090151	
38.1	0.00011256	0.97416186	
38.3	0.00013320	0.97696813	
38.5	0.00015729	0.97940058	
38.7	0.00018538	0.98152172	
38.9	0.00021808	0.98338079	
39.1	0.00025606	0.98501739	
39.3	0.00030012	0.98646377	
39.5	0.00035114	0.98774640	
39.7	0.00041014	0.98888734	
39.9	0.00047824	0.98990507	
40.0	0.00051610	0.99037269	
41.0	0.00108210	0.99389273	
42.0	0.00218680	0.99601103	
43.0	0.00427248	0.99733267	
43.5	0.00590156	0.99780250	
44.0	0.00809082	0.99818149	
45.0	0.01488383	0.99874048	
46.0	0.02665070	0.99911717	
47.0	0.04653107	0.99937682	
48.0	0.07934573	0.99956013	
49.0	0.13233871	0.99969262	
50.0	0.21617997	0.99979189	
51.0	0.34629320	0.99986790	
52.0	0.54459289	0.99992936	
52.2	0.59543491	0.99999987	
52.4	0.64666624	0.99999982	
52.6	0.70912234	0.99999911	
52.8	0.77164947	0.99999968	
53.0	0.84176331	0.99999444	
53.2	0.91637497	0.99999969	
53.4068	1	1	

S1S2

	solid S1	*solid S2*	
T [K]	*wCH4*	*xCH4*	
36.0	0.03097803	0.95911737	
36.2	0.03174852	0.95816628	
36.4	0.03253157	0.95720115	
36.6	0.03332728	0.95622191	
36.8	0.03413576	0.95522846	
37.0	0.03495715	0.95422070	
37.1797	**0.03570637**	**0.95330248**	**VS1S2**

VS1

	vapor	*solid S1*	
T [K]	*yCH4*	*wCH4*	
37.1279	0	0	
37.1797	**0.00005041**	**0.03570637**	**VS1S2**

Figure 2

VS2

(deposition points)

0.3 mole% methane

T [K]	*P [μbar]*
41.4	6.1598
41.5	6.6080
41.6	7.0864
41.7	7.5968
41.8	8.1412
41.9	8.7217
42.0	9.3404
42.1	9.9998
42.2	10.7021
42.3	11.4501
42.4	12.2463
42.5	13.0937
42.6	13.9952
42.7	14.9540
42.8	15.9735

0.6 mole% methane

T [K]	*P [μbar]*
42.4	6.1331
42.5	6.5577
42.6	7.0095
42.7	7.4901
42.8	8.0012
42.9	8.5444
43.0	9.1216
43.1	9.7349
43.2	10.3862
43.3	11.0777
43.4	11.8117
43.5	12.5905
43.6	13.4167
43.7	14.2928
43.8	15.2217

VS1S2

(three-phase equilibrium)

T [K]	*P [μbar]*
36.4	7.9074
36.5	8.4213
36.6	8.9654
36.7	9.5412
36.8	10.1505
36.9	10.7950
37.0	11.4765
37.1	12.1968
37.2	12.9579
37.3	13.7620
37.4	14.6110
37.5	15.5074

VS1

(sublimation point)

0.3 mole% methane

T [K]	*P [μbar]*
36.4	8.0797
36.5	8.6053
36.6	9.1646
36.7	9.7633
36.8	10.3855
36.9	11.0528
37.0	11.7561
37.1	12.5009
37.2	13.2815
37.3	14.1135
37.4	14.9887
37.5	15.9116

Scenario 2

(PT profile h > 2 km)

T [K]	*P [μbar]*
37.00	11.4574
37.19	11.3930
37.39	11.3294
37.59	11.2664
37.78	11.2042
37.98	11.1426
38.18	11.0817
38.39	11.0214
38.59	10.9618
38.80	10.9029
39.02	10.8446
39.24	10.7870
39.47	10.7300
39.70	10.6736
39.94	10.6179
40.18	10.5628
40.44	10.5084
40.70	10.4546
40.97	10.4014
41.25	10.3489
41.54	10.2971
41.84	10.2459
42.15	10.1954
42.48	10.1455
42.82	10.0963
43.15	10.0502

Figure 3b

Isobaric at 10.2 μbar

For Fig. 3a, isobaric at 12.8 μbar, see the data of Fig. 1b.

VS2

T [K]	*vapor yCH4*	*solid S2 xCH4*	
36.8079	**0.0000456**	**0.9551887**	**VS1S2**
36.9	0.0000496	0.9580628	
37.0	0.0000543	0.9608954	
37.1	0.0000595	0.9634665	
37.2	0.0000650	0.9658110	
37.3	0.0000711	0.9679557	
37.4	0.0000777	0.9699250	
37.5	0.0000848	0.9717379	
37.6	0.0000925	0.9734106	
37.7	0.0001009	0.9749580	
37.8	0.0001100	0.9763922	
37.9	0.0001198	0.9777239	
38.0	0.0001305	0.9789626	
38.1	0.0001420	0.9801166	
38.2	0.0001545	0.9811933	
38.3	0.0001679	0.9821990	
38.4	0.0001825	0.9831398	
38.5	0.0001982	0.9840207	
38.6	0.0002152	0.9848464	
38.7	0.0002335	0.9856216	
38.8	0.0002533	0.9863493	
38.9	0.0002746	0.9870336	
39.0	0.0002976	0.9876773	
39.1	0.0003223	0.9882835	
39.2	0.0003490	0.9888548	
39.3	0.0003777	0.9893935	
39.4	0.0004085	0.9899019	
39.5	0.0004418	0.9903819	
39.6	0.0004775	0.9908354	
39.7	0.0005158	0.9912639	
39.8	0.0005571	0.9916698	
39.9	0.0006014	0.9920538	
40.0	0.0006489	0.9924172	
40.1	0.0007000	0.9927614	
40.2	0.0007547	0.9930880	
40.3	0.0008134	0.9933976	
40.4	0.0008764	0.9936913	
40.5	0.0009438	0.9939701	
40.6	0.0010160	0.9942349	
40.7	0.0010934	0.9944864	
40.8	0.0011762	0.9947253	
40.9	0.0012648	0.9949525	
41.0	0.0013596	0.9951687	
41.1	0.0014610	0.9953744	
41.2	0.0015693	0.9955700	
41.3	0.0016851	0.9957563	
41.4	0.0018088	0.9959339	
41.5	0.0019409	0.9961027	
41.6	0.0020818	0.9962640	
41.7	0.0022323	0.9964176	
41.8	0.0023928	0.9965641	
41.9	0.0025640	0.9967040	
42.0	0.0027465	0.9968372	
42.1	0.0029409	0.9969647	
42.2	0.0031481	0.9970859	
42.3	0.0033689	0.9972019	
42.4	0.0036038	0.9973129	
42.5	0.0038539	0.9974189	
42.6	0.0041200	0.9975202	
42.7	0.0044032	0.9976170	
42.8	0.0047042	0.9977096	
42.9	0.0050243	0.9977982	
43.0	0.0053645	0.9978830	
43.1	0.0057259	0.9979641	
43.2	0.0061098	0.9980417	
43.3	0.0065173	0.9981161	
43.4	0.0069500	0.9981874	
43.5	0.0074092	0.9982556	
43.6	0.0078964	0.9983209	
43.7	0.0084130	0.9983837	
43.8	0.0089609	0.9984438	
43.9	0.0095416	0.9985012	
44.0	0.0101569	0.9985563	
44.5	0.0138234	0.9988015	
45.0	0.0186826	0.9990015	
45.5	0.0250794	0.9991660	
46.0	0.0334501	0.9993020	
46.5	0.0443329	0.9994152	
47.0	0.0583986	0.9995102	
47.5	0.0764774	0.9995896	
48.0	0.0995809	0.9996572	
48.5	0.1289492	0.9997150	
49.0	0.1660884	0.9997647	
49.5	0.2128087	0.9998080	
50.0	0.2712963	0.9998457	
50.5	0.3458747	0.9999992	
51.0	0.4347997	0.9999985	
51.5	0.5464853	0.9999998	
52.0	0.6837161	0.9999997	
52.5	0.8513040	0.9999997	
52.8721	1	1	

S1S2

T [K]	*solid S1 wCH4*	*solid S2 xCH4*	
36.5	0.0329278	0.9567133	
36.6	0.0333273	0.9562219	
36.7	0.0337299	0.9557270	
36.8079	**0.0341680**	**0.9551887**	**VS1S2**

VS1

T [K]	*vapor yCH4*	*solid S1 wCH4*	
36.7591	0	0	
36.8079	**0.0000456**	**0.0341680**	**VS1S2**

Figure 4a – 4b

Scenario 1: Two-phase VS2 flash calculations at T (according to gradient) and P (hydrostatic pressure)
The density ρ is the total density of all phases

0.3 mole% methane			*In vapor*	*In solidS2*	
h [km]	*P [μbar]*	*ρ [μmol/L]*	*yCH4*	*xN2*	*σ*
0.0	12.7872	3.9650	0.000218	0.016614	0.002830
0.1	12.7187	3.9274	0.000249	0.015199	0.002794
0.2	12.6509	3.8951	0.000274	0.014260	0.002766
0.3	12.5836	3.8671	0.000292	0.013663	0.002746
0.4	12.5168	3.8427	0.000303	0.013321	0.002734
0.5	12.4504	3.8213	0.000307	0.013175	0.002730
0.6	12.3843	3.8023	0.000306	0.013186	0.002731
0.7	12.3186	3.7852	0.000300	0.013323	0.002738
0.8	12.2531	3.7696	0.000290	0.013562	0.002748
0.9	12.1879	3.7551	0.000279	0.013882	0.002760
1.0	12.1230	3.7414	0.000266	0.014265	0.002774
1.1	12.0583	3.7280	0.000253	0.014693	0.002788
1.2	11.9939	3.7149	0.000241	0.015150	0.002802
1.3	11.9297	3.7017	0.000229	0.015617	0.002816
1.4	11.8657	3.6882	0.000218	0.016075	0.002828
1.5	11.8020	3.6743	0.000208	0.016505	0.002839
1.6	11.7386	3.6597	0.000200	0.016890	0.002848
1.7	11.6754	3.6444	0.000194	0.017210	0.002856
1.8	11.6125	3.6283	0.000189	0.017448	0.002861
1.9	11.5499	3.6112	0.000186	0.017590	0.002865
2.0	11.4876	3.5931	0.000185	0.017624	0.002866
2.1	11.4256	3.5739	0.000186	0.017542	0.002865
2.2	11.3640	3.5537	0.000188	0.017339	0.002862
2.3	11.3028	3.5323	0.000193	0.017014	0.002856
2.4	11.2419	3.5098	0.000200	0.016573	0.002847
2.5	11.1815	3.4862	0.000210	0.016024	0.002836
2.6	11.1215	3.4614	0.000223	0.015378	0.002821
2.7	11.0619	3.4356	0.000240	0.014649	0.002802
2.8	11.0028	3.4086	0.000261	0.013854	0.002778
2.9	10.9442	3.3807	0.000287	0.013008	0.002750
3.0	10.8861	3.3517	0.000319	0.012130	0.002715
3.1	10.8285	3.3217	0.000359	0.011234	0.002672
3.2	10.7714	3.2908	0.000409	0.010337	0.002620
3.3	10.7149	3.2590	0.000470	0.009451	0.002555
3.4	10.6590	3.2264	0.000547	0.008589	0.002476
3.5	10.6036	3.1929	0.000642	0.007759	0.002378
3.6	10.5488	3.1586	0.000762	0.006969	0.002255
3.7	10.4947	3.1236	0.000913	0.006226	0.002102
3.8	10.4411	3.0878	0.001105	0.005532	0.001907
3.9	10.3882	3.0513	0.001350	0.004890	0.001660
4.0	10.3359	3.0140	0.001664	0.004300	0.001344
4.1	10.2843	2.9760	0.002069	0.003763	0.000937
4.2	10.2334	2.9371	0.002594	0.003278	0.000409
4.262	10.2021	2.9126	0.003	0.003	0

0.6 mole% methane			*In vapor*	*In solidS2*	
h [km]	*P [μbar]*	*ρ [μmol/L]*	*yCH4*	*xN2*	*σ*
0.0	12.7884	3.9775	0.000218	0.016616	0.005881
0.1	12.7198	3.9398	0.000249	0.015201	0.005841
0.2	12.6519	3.9073	0.000274	0.014261	0.005810
0.3	12.5844	3.8792	0.000292	0.013664	0.005788
0.4	12.5175	3.8547	0.000303	0.013321	0.005776
0.5	12.4509	3.8331	0.000307	0.013176	0.005771
0.6	12.3848	3.8141	0.000306	0.013187	0.005772
0.7	12.3189	3.7969	0.000300	0.013324	0.005779
0.8	12.2533	3.7812	0.000290	0.013562	0.005790
0.9	12.1880	3.7666	0.000279	0.013882	0.005803
1.0	12.1230	3.7528	0.000266	0.014265	0.005818
1.1	12.0582	3.7394	0.000253	0.014693	0.005834
1.2	11.9937	3.7262	0.000241	0.015150	0.005849
1.3	11.9293	3.7129	0.000229	0.015616	0.005864
1.4	11.8653	3.6994	0.000218	0.016074	0.005878
1.5	11.8015	3.6854	0.000208	0.016504	0.005890
1.6	11.7379	3.6707	0.000200	0.016889	0.005900
1.7	11.6746	3.6554	0.000194	0.017208	0.005909
1.8	11.6116	3.6391	0.000189	0.017447	0.005915
1.9	11.5489	3.6220	0.000186	0.017589	0.005919
2.0	11.4865	3.6038	0.000185	0.017623	0.005920
2.1	11.4244	3.5846	0.000186	0.017540	0.005919
2.2	11.3627	3.5642	0.000188	0.017336	0.005915
2.3	11.3014	3.5427	0.000193	0.017012	0.005909
2.4	11.2404	3.5201	0.000200	0.016571	0.005899
2.5	11.1799	3.4964	0.000210	0.016022	0.005885
2.6	11.1198	3.4715	0.000223	0.015375	0.005868
2.7	11.0601	3.4455	0.000240	0.014647	0.005847
2.8	11.0009	3.4185	0.000261	0.013851	0.005821
2.9	10.9422	3.3904	0.000287	0.013006	0.005790
3.0	10.8840	3.3613	0.000319	0.012127	0.005752
3.1	10.8263	3.3312	0.000359	0.011232	0.005707
3.2	10.7691	3.3002	0.000409	0.010334	0.005652
3.3	10.7126	3.2682	0.000470	0.009449	0.005585
3.4	10.6565	3.2354	0.000547	0.008587	0.005504
3.5	10.6011	3.2018	0.000642	0.007757	0.005403
3.6	10.5462	3.1674	0.000762	0.006968	0.005278
3.7	10.4920	3.1323	0.000914	0.006224	0.005123
3.8	10.4383	3.0963	0.001106	0.005530	0.004927
3.9	10.3854	3.0597	0.001350	0.004888	0.004679
4.0	10.3330	3.0223	0.001664	0.004299	0.004362
4.1	10.2813	2.9841	0.002069	0.003762	0.003954
4.2	10.2303	2.9451	0.002595	0.003277	0.003425
4.3	10.1800	2.9053	0.003281	0.002841	0.002736
4.4	10.1304	2.8645	0.004181	0.002451	0.001831
4.5	10.0814	2.8226	0.005371	0.002105	0.000633
4.543	10.0606	2.8042	0.006	0.001969	0

Figure 5a – 5b

Scenario 2: Three-phase VS1S2 calculations along the VSS curve below 2 km, and VS2 above it
The density ρ is the total density of all phases

0.3 mole% methane			*In vapor*	*In solidS2*	
h [km]	*P [μbar]*	*ρ [μmol/L]*	*yCH4*	*xN2*	*σ*
0.0	12.8253	4.1614	0.000050	0.046714	0.003094
0.1	12.7533	4.1390	0.000050	0.046666	0.003094
0.2	12.6817	4.1168	0.000050	0.046619	0.003094
0.3	12.6105	4.0947	0.000050	0.046571	0.003094
0.4	12.5397	4.0728	0.000050	0.046523	0.003094
0.5	12.4693	4.0509	0.000050	0.046475	0.003094
0.6	12.3992	4.0292	0.000050	0.046428	0.003094
0.7	12.3296	4.0076	0.000050	0.046380	0.003094
0.8	12.2604	3.9860	0.000049	0.046333	0.003094
0.9	12.1915	3.9646	0.000049	0.046285	0.003094
1.0	12.1230	3.9434	0.000049	0.046238	0.003094
1.1	12.0549	3.9222	0.000049	0.046191	0.003094
1.2	11.9872	3.9011	0.000049	0.046143	0.003094
1.3	11.9198	3.8802	0.000049	0.046096	0.003094
1.4	11.8528	3.8593	0.000049	0.046049	0.003094
1.5	11.7862	3.8386	0.000049	0.046002	0.003094
1.6	11.7200	3.8180	0.000048	0.045955	0.003094
1.7	11.6541	3.7975	0.000048	0.045908	0.003094
1.8	11.5886	3.7771	0.000048	0.045861	0.003094
1.9	11.5234	3.7568	0.000048	0.045814	0.003094
2.0	11.4586	3.7366	0.000048	0.045767	0.003094
2.1	11.3944	3.6959	0.000058	0.039559	0.003064
2.2	11.3308	3.6559	0.000069	0.034471	0.003036
2.3	11.2680	3.6165	0.000083	0.030221	0.003009
2.4	11.2058	3.5777	0.000098	0.026618	0.002981
2.5	11.1443	3.5393	0.000117	0.023527	0.002952
2.6	11.0835	3.5014	0.000140	0.020849	0.002921
2.7	11.0234	3.4638	0.000167	0.018512	0.002887
2.8	10.9639	3.4265	0.000199	0.016459	0.002848
2.9	10.9050	3.3894	0.000238	0.014645	0.002804
3.0	10.8468	3.3526	0.000284	0.013035	0.002753
3.1	10.7893	3.3159	0.000340	0.011602	0.002692
3.2	10.7324	3.2793	0.000409	0.010322	0.002620
3.3	10.6761	3.2428	0.000492	0.009177	0.002533
3.4	10.6205	3.2063	0.000593	0.008151	0.002428
3.5	10.5655	3.1698	0.000718	0.007231	0.002300
3.6	10.5111	3.1332	0.000873	0.006405	0.002143
3.7	10.4574	3.0965	0.001064	0.005664	0.001949
3.8	10.4043	3.0597	0.001303	0.004999	0.001708
3.9	10.3519	3.0226	0.001601	0.004404	0.001407
4.0	10.3001	2.9853	0.001977	0.003870	0.001029
4.1	10.2490	2.9477	0.002451	0.003394	0.000552
4.192	10.2026	2.9127	0.003	0.003	0

0.6 mole% methane			*In vapor*	*In solidS2*	
h [km]	*P [μbar]*	*ρ [μmol/L]*	*yCH4*	*xN2*	*σ*
0.0	12.8266	4.1750	0.000050	0.046715	0.006241
0.1	12.7545	4.1525	0.000050	0.046667	0.006241
0.2	12.6828	4.1302	0.000050	0.046619	0.006241
0.3	12.6114	4.1080	0.000050	0.046572	0.006241
0.4	12.5405	4.0859	0.000050	0.046524	0.006241
0.5	12.4699	4.0639	0.000050	0.046476	0.006241
0.6	12.3998	4.0421	0.000050	0.046428	0.006240
0.7	12.3300	4.0204	0.000050	0.046381	0.006240
0.8	12.2606	3.9987	0.000049	0.046333	0.006240
0.9	12.1916	3.9772	0.000049	0.046285	0.006240
1.0	12.1230	3.9558	0.000049	0.046238	0.006240
1.1	12.0548	3.9346	0.000049	0.046191	0.006239
1.2	11.9869	3.9134	0.000049	0.046143	0.006239
1.3	11.9194	3.8923	0.000049	0.046096	0.006239
1.4	11.8523	3.8714	0.000049	0.046048	0.006239
1.5	11.7856	3.8505	0.000049	0.046001	0.006239
1.6	11.7192	3.8298	0.000048	0.045954	0.006239
1.7	11.6532	3.8092	0.000048	0.045907	0.006238
1.8	11.5876	3.7887	0.000048	0.045860	0.006238
1.9	11.5223	3.7683	0.000048	0.045813	0.006238
2.0	11.4574	3.7480	0.000048	0.045766	0.006238
2.1	11.3930	3.7071	0.000058	0.039553	0.006187
2.2	11.3294	3.6669	0.000069	0.034465	0.006143
2.3	11.2664	3.6273	0.000083	0.030216	0.006102
2.4	11.2042	3.5882	0.000099	0.026613	0.006063
2.5	11.1426	3.5497	0.000117	0.023522	0.006025
2.6	11.0817	3.5116	0.000140	0.020845	0.005986
2.7	11.0214	3.4738	0.000167	0.018508	0.005944
2.8	10.9618	3.4363	0.000199	0.016455	0.005899
2.9	10.9029	3.3991	0.000238	0.014642	0.005849
3.0	10.8446	3.3621	0.000284	0.013032	0.005793
3.1	10.7870	3.3253	0.000340	0.011599	0.005728
3.2	10.7300	3.2886	0.000409	0.010320	0.005652
3.3	10.6736	3.2519	0.000492	0.009175	0.005562
3.4	10.6179	3.2153	0.000594	0.008149	0.005454
3.5	10.5628	3.1786	0.000719	0.007229	0.005324
3.6	10.5084	3.1419	0.000873	0.006403	0.005165
3.7	10.4546	3.1051	0.001065	0.005663	0.004969
3.8	10.4014	3.0681	0.001303	0.004998	0.004727
3.9	10.3489	3.0309	0.001602	0.004402	0.004425
4.0	10.2971	2.9935	0.001977	0.003869	0.004046
4.1	10.2459	2.9557	0.002452	0.003393	0.003569
4.2	10.1954	2.9175	0.003054	0.002967	0.002964
4.3	10.1455	2.8788	0.003822	0.002588	0.002193
4.4	10.0963	2.8395	0.004805	0.002252	0.001203
4.495	10.0502	2.8014	0.006	0.001967	0

Figure A1

Temperature profile
Correlated over the data by Hinson et al. (2017)
Eq (A1) - (ingress/sunset case)

h [km]	*T [K]*	*h [km]*	*T [K]*
0.0	38.899	2.9	39.042
0.1	39.059	3.0	39.170
0.2	39.172	3.1	39.312
0.3	39.245	3.2	39.470
0.4	39.284	3.3	39.643
0.5	39.294	3.4	39.832
0.6	39.281	3.5	40.037
0.7	39.249	3.6	40.257
0.8	39.202	3.7	40.493
0.9	39.145	3.8	40.746
1.0	39.080	3.9	41.014
1.1	39.011	4.0	41.299
1.2	38.941	4.1	41.601
1.3	38.871	4.2	41.920
1.4	38.804	4.3	42.256
1.5	38.743	4.4	42.610
1.6	38.688	4.5	42.982
1.7	38.641	4.6	43.375
1.8	38.604	4.7	43.785
1.9	38.578	4.8	44.214
2.0	38.563	4.9	44.663
2.1	38.561	5.0	45.133
2.2	38.571	5.1	45.625
2.3	38.595	5.2	46.137
2.4	38.633	5.3	46.673
2.5	38.685	5.4	47.231
2.6	38.752	5.5	47.813
2.7	38.834	5.6	48.418
2.8	38.931		

For Scenario 2
Correlated over the data by Hinson et al. (2017)
Eq (A2) for h > 2 km and VSS for h < 2 km

h [km]	*T [K]*	*h [km]*	*T [K]*
0.0	37.183	2.4	37.784
0.1	37.174	2.5	37.983
0.2	37.164	2.6	38.184
0.3	37.155	2.7	38.387
0.4	37.146	2.8	38.594
0.5	37.137	2.9	38.805
0.6	37.127	3.0	39.020
0.7	37.118	3.1	39.240
0.8	37.109	3.2	39.466
0.9	37.099	3.3	39.697
1.0	37.090	3.4	39.936
1.1	37.081	3.5	40.182
1.2	37.071	3.6	40.435
1.3	37.062	3.7	40.697
1.4	37.053	3.8	40.968
1.5	37.044	3.9	41.249
1.6	37.034	4.0	41.540
1.7	37.025	4.1	41.842
1.8	37.016	4.2	42.155
1.9	37.007	4.3	42.479
2.0	36.997	4.4	42.817
2.1	37.194	4.495	43.149
2.2	37.390		
2.3	37.586		

Figure A2

VS2 (related to Fig. 4)
Two-phase flash calculations at T (according to gradient) and P (hydrostatic pressure)

0.3 mole% methane					*0.6 mole% methane*				
h [km]	*T [K]*	*P [μbar]*	*γN2 in S2*	*γCH4 in S2*	*h [km]*	*T [K]*	*P [μbar]*	*γN2 in S2*	*γCH4 in S2*
0.0	38.898	12.78718	21.486	1.000813	0.0	38.898	12.78839	21.486	1.000808
0.1	39.058	12.71873	21.386	1.000676	0.1	39.058	12.71981	21.386	1.000672
0.2	39.172	12.65090	21.308	1.000590	0.2	39.172	12.65186	21.308	1.000590
0.3	39.245	12.58361	21.257	1.000540	0.3	39.245	12.58444	21.257	1.000540
0.4	39.284	12.51678	21.233	1.000515	0.4	39.284	12.51748	21.233	1.000515
0.5	39.294	12.45035	21.234	1.000501	0.5	39.294	12.45094	21.234	1.000505
0.6	39.281	12.38429	21.254	1.000504	0.6	39.281	12.38476	21.254	1.000504
0.7	39.249	12.31855	21.292	1.000517	0.7	39.249	12.31890	21.292	1.000514
0.8	39.202	12.25310	21.342	1.000534	0.8	39.202	12.25333	21.342	1.000534
0.9	39.145	12.18792	21.400	1.000559	0.9	39.145	12.18804	21.400	1.000562
1.0	39.080	12.12300	21.464	1.000589	1.0	39.080	12.12300	21.464	1.000589
1.1	39.011	12.05832	21.530	1.000630	1.1	39.011	12.05821	21.530	1.000630
1.2	38.940	11.99388	21.596	1.000672	1.2	38.940	11.99365	21.596	1.000672
1.3	38.871	11.92968	21.659	1.000715	1.3	38.871	11.92934	21.659	1.000715
1.4	38.804	11.86572	21.718	1.000755	1.4	38.804	11.86527	21.718	1.000759
1.5	38.742	11.80201	21.772	1.000803	1.5	38.742	11.80145	21.772	1.000803
1.6	38.688	11.73855	21.820	1.000839	1.6	38.688	11.73788	21.820	1.000844
1.7	38.641	11.67537	21.862	1.000877	1.7	38.641	11.67459	21.862	1.000872
1.8	38.604	11.61246	21.898	1.000899	1.8	38.604	11.61158	21.898	1.000899
1.9	38.578	11.54986	21.927	1.000913	1.9	38.578	11.54886	21.927	1.000913
2.0	38.563	11.48757	21.949	1.000919	2.0	38.563	11.48647	21.949	1.000919
2.1	38.561	11.42561	21.964	1.000911	2.1	38.561	11.42440	21.964	1.000911
2.2	38.571	11.36400	21.971	1.000888	2.2	38.571	11.36269	21.971	1.000888
2.3	38.595	11.30276	21.969	1.000851	2.3	38.595	11.30135	21.969	1.000856
2.4	38.633	11.24191	21.957	1.000811	2.4	38.633	11.24040	21.958	1.000811
2.5	38.686	11.18147	21.934	1.000754	2.5	38.686	11.17986	21.934	1.000754
2.6	38.752	11.12146	21.897	1.000693	2.6	38.752	11.11975	21.897	1.000693
2.7	38.834	11.06189	21.844	1.000629	2.7	38.834	11.06009	21.844	1.000629
2.8	38.931	11.00279	21.774	1.000560	2.8	38.931	11.00089	21.774	1.000564
2.9	39.043	10.94418	21.684	1.000492	2.9	39.043	10.94218	21.684	1.000492
3.0	39.170	10.88606	21.573	1.000427	3.0	39.170	10.88398	21.573	1.000427
3.1	39.313	10.82847	21.439	1.000364	3.1	39.313	10.82629	21.439	1.000366
3.2	39.471	10.77141	21.281	1.000308	3.2	39.471	10.76914	21.282	1.000308
3.3	39.644	10.71490	21.099	1.000257	3.3	39.644	10.71255	21.100	1.000257
3.4	39.833	10.65895	20.892	1.000210	3.4	39.833	10.65651	20.893	1.000210
3.5	40.038	10.60359	20.661	1.000170	3.5	40.038	10.60106	20.661	1.000170
3.6	40.258	10.54881	20.405	1.000137	3.6	40.258	10.54621	20.405	1.000137
3.7	40.495	10.49465	20.126	1.000109	3.7	40.495	10.49196	20.126	1.000109
3.8	40.747	10.44110	19.824	1.000085	3.8	40.747	10.43834	19.824	1.000085
3.9	41.016	10.38819	19.502	1.000066	3.9	41.016	10.38535	19.502	1.000065
4.0	41.301	10.33592	19.161	1.000051	4.0	41.301	10.33300	19.161	1.000051
4.1	41.603	10.28431	18.802	1.000039	4.1	41.603	10.28132	18.802	1.000039
4.2	41.922	10.23337	18.428	1.000030	4.2	41.922	10.23030	18.428	1.000029
4.262	42.128	10.20213	18.189	1.000026	4.3	42.258	10.17997	18.040	1.000022
					4.4	42.612	10.13035	17.641	1.000017
					4.5	42.984	10.08144	17.231	1.000012
					4.543	43.150	10.06063	17.053	1.000010

Figure A3

VS1S2 T [K]	P [μbar]	γN2 in S2	γCH4 in S1	T [K]	P [μbar]	γN2 in S2	γCH4 in S1
35.4	4.1290	25.568	33.625	40.3	72.5576	14.834	18.753
35.5	4.4136	25.260	33.191	40.4	76.3547	14.683	18.548
35.6	4.7161	24.957	32.764	40.5	80.3294	14.535	18.347
35.7	5.0374	24.658	32.344	40.6	84.4891	14.388	18.148
35.8	5.3786	24.365	31.931	40.7	88.8413	14.243	17.953
35.9	5.7407	24.076	31.525	40.8	93.3937	14.100	17.759
36.0	6.1249	23.791	31.126	40.9	98.1545	13.959	17.569
36.1	6.5323	23.511	30.733	41.0	103.1319	13.820	17.381
36.2	6.9644	23.236	30.347	41.1	108.3345	13.683	17.195
36.3	7.4223	22.965	29.967	41.2	113.7713	13.547	17.012
36.4	7.9074	22.697	29.594	41.3	119.4514	13.413	16.832
36.5	8.4213	22.434	29.226	41.4	125.3843	13.281	16.654
36.6	8.9654	22.175	28.864	41.5	131.5799	13.150	16.478
36.7	9.5412	21.920	28.508	41.6	138.0483	13.021	16.305
36.8	10.1505	21.669	28.158	41.7	144.7999	12.894	16.134
36.9	10.7950	21.422	27.814	41.8	151.8455	12.768	15.965
37.0	11.4765	21.178	27.474	41.9	159.1962	12.644	15.798
37.1	12.1968	20.938	27.141	42.0	166.8637	12.521	15.634
37.2	12.9579	20.702	26.812	42.1	174.8596	12.400	15.472
37.3	13.7620	20.469	26.489	42.2	183.1963	12.281	15.312
37.4	14.6110	20.239	26.170	42.3	191.8863	12.163	15.154
37.5	15.5074	20.013	25.857	42.4	200.9426	12.046	14.998
37.6	16.4533	19.790	25.548	42.5	210.3787	11.931	14.844
37.7	17.4513	19.571	25.245	42.6	220.2083	11.817	14.692
37.8	18.5038	19.355	24.945	42.7	230.4456	11.704	14.542
37.9	19.6135	19.142	24.651	42.8	241.1054	11.593	14.393
38.0	20.7833	18.931	24.361	42.9	252.2027	11.483	14.247
38.1	22.0158	18.724	24.075	43.0	263.7530	11.375	14.103
38.2	23.3142	18.520	23.794	43.1	275.7724	11.268	13.960
38.3	24.6815	18.319	23.517	43.2	288.2772	11.162	13.819
38.4	26.1209	18.121	23.244	43.3	301.2845	11.057	13.680
38.5	27.6359	17.925	22.975	43.4	314.8117	10.954	13.543
38.6	29.2299	17.733	22.710	43.5	328.8766	10.852	13.407
38.7	30.9065	17.543	22.449	43.6	343.4979	10.751	13.273
38.8	32.6696	17.355	22.192	43.7	358.6943	10.651	13.141
38.9	34.5231	17.171	21.939	43.8	374.4855	10.552	13.010
39.0	36.4710	16.988	21.689	43.9	390.8915	10.455	12.881
39.1	38.5176	16.809	21.443	44.0	407.9329	10.358	12.754
39.2	40.6673	16.631	21.201	44.1	425.6308	10.263	12.628
39.3	42.9247	16.457	20.962	44.2	444.0071	10.169	12.504
39.4	45.2945	16.284	20.726	44.3	463.0840	10.076	12.381
39.5	47.7817	16.114	20.494	44.4	482.8846	9.984	12.259
39.6	50.3913	15.947	20.266	44.5	503.4323	9.893	12.140
39.7	53.1287	15.781	20.040	44.6	524.7515	9.803	12.021
39.8	55.9993	15.618	19.818	44.7	546.8669	9.714	11.904
39.9	59.0088	15.457	19.599	44.8	569.8041	9.626	11.788
40.0	62.1632	15.298	19.383	44.9	593.5892	9.539	11.674
40.1	65.4685	15.141	19.170	45.0	618.2491	9.453	11.561
40.2	68.9311	14.987	18.960				